AD-A192 909 STUDY OF THE INFLUENCE OF METALLURGICAL FACTORS ON FATIGUE AND FRACTURE O..(U) SOUTHWEST RESEARCH INST SAN ANTONIO TX J LANKFORD ET AL. 31 JAN 88 SWRI-06-8972/2 1/1

UNCLASSIFIED AFOSR-TR-88-0294 F49620-86-C-0024 F/G 11/6.1 NL

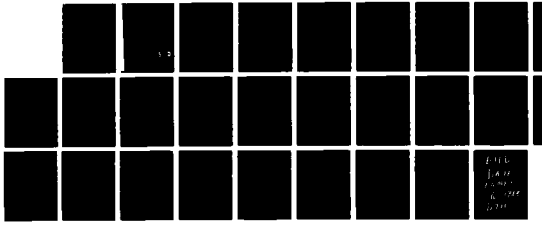

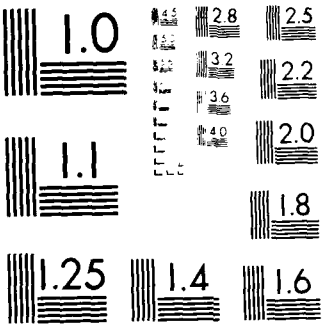

(2)

STUDY OF THE INFLUENCE OF METALLURGICAL FACTORS ON FATIGUE AND FRACTURE OF AEROSPACE STRUCTURAL MATERIALS

By
James Lankford
David L. Davidson
Kwai S. Chan
Gerald R. Leverant

AFOSR ANNUAL REPORT

This research was sponsored by the Air Force Office of Scientific Research,
Electronic and Materials Sciences Directorate
Under Contract F49620-86-C-0024

Approved for release; distribution unlimited.

January 1988

SOUTHWEST RESEARCH INSTITUTE
SAN ANTONIO HOUSTON

SOUTHWEST RESEARCH INSTITUTE
Post Office Drawer 28510, 6220 Culebra Road
San Antonio, Texas 78284

STUDY OF THE INFLUENCE OF METALLURGICAL FACTORS ON FATIGUE AND FRACTURE OF AEROSPACE STRUCTURAL MATERIALS

By
James Lankford
David L. Davidson
Kwai S. Chan
Gerald R. Leverant

AFOSR ANNUAL REPORT

This research was sponsored by the Air Force Office of Scientific Research,
Electronic and Materials Sciences Directorate
Under Contract F49620-86-C-0024

Approved for release; distribution unlimited.

January 1988

Approved:

Ulric S. Lindholm, Vice President
Engineering and Materials Sciences Division

UNCLASSIFIED

SECURITY CLASSIFICATION OF THIS PAGE

REPORT DOCUMENTATION PAGE

1a. REPORT SECURITY CLASSIFICATION UNCLASSIFIED	1b. RESTRICTIVE MARKINGS
2a. SECURITY CLASSIFICATION AUTHORITY	3. DISTRIBUTION/AVAILABILITY OF REPORT Approved for public release; distribution unlimited
2b. DECLASSIFICATION/DOWNGRADING SCHEDULE	
4. PERFORMING ORGANIZATION REPORT NUMBER(S) 06-8972	5. MONITORING ORGANIZATION REPORT NUMBER(S) AFOSR-TR- 88-0294
6a. NAME OF PERFORMING ORGANIZATION Southwest Research Institute 6b. OFFICE SYMBOL (If applicable)	7a. NAME OF MONITORING ORGANIZATION Air Force Office of Scientific Research
6c. ADDRESS (City, State, and ZIP Code) 6220 Culebra Road San Antonio, TX 78284	7b. ADDRESS (City, State, and ZIP Code) Department of the Air Force Bolling Air Force Base Washington, D.C. 20332
8a. NAME OF FUNDING/SPONSORING ORGANIZATION AFOSR 8b. OFFICE SYMBOL (If applicable)	9. PROCUREMENT INSTRUMENT IDENTIFICATION NUMBER
8c. ADDRESS (City, State, and ZIP Code) Department of the Air Force Bolling Air Force Base Washington, D.C. 20332	10. SOURCE OF FUNDING NUMBERS PROGRAM ELEMENT NO. 61102F; PROJECT NO. 2306; TASK NO. A1; WORK UNIT ACCESSION NO.

11. TITLE (Include Security Classification)
Study of the Influence of Microstructural Factors on Fatigue and Fracture of Aerospace Structural Materials

12. PERSONAL AUTHOR(S)
J. Lankford, D.L. Davidson, G.R. Leverant, K.S. Chan

13a. TYPE OF REPORT	13b. TIME COVERED	14. DATE OF REPORT (Year, Month, Day)	15. PAGE COUNT
Annual Report	FROM 1/1/87 TO 12/31/87	88/01/31	

16. SUPPLEMENTARY NOTATION

17 COSATI CODES			18. SUBJECT TERMS (Continue on reverse if necessary and identify by block number)
FIELD	GROUP	SUB-GROUP	ALUMINUM; ALUMINUM-IRON-X

This report summarizes the results of a two-phase study involving (1) experimental characterization and analytical modeling of fatigue crack tip micromechanics in aerospace structural Al alloys, and (2) identification and modeling of key microstructural factors controlling fracture in Al-Fe-X alloys.

Dynamic load cycling within the SEM and stereoimaging strain analysis have been used to characterize crack opening loads, strains, and effective stress intensity (ΔK_{eff}) values for

DELTA

(continued)

20. DISTRIBUTION/AVAILABILITY OF ABSTRACT	21. ABSTRACT SECURITY CLASSIFICATION
☒ UNCLASSIFIED/UNLIMITED ☐ SAME AS RPT ☐ DTIC USERS	Unclassified
22a. NAME OF RESPONSIBLE INDIVIDUAL B Kennedy	22b. TELEPHONE (Include Area Code) 202-767-4933
	22c. OFFICE SYMBOL NE

DD FORM 1473, 84 MAR 83 APR edition may be used until exhausted. All other editions are obsolete.

SECURITY CLASSIFICATION OF THIS PAGE
UNCLASSIFIED

19. Abstract (continued)

large and small cracks in a variety of alloys; both constant amplitude and overload/underload situations were studied. It was found that ΔK_{eff} based on local crack tip opening load was not an adequate crack growth rate correlating factor. Instead, it was necessary to use a new driving force term ΔK^{*}_{eff}, which includes both closure and local crack tip plasticity. The latter was computed by calculating ΔJ integrals within the crack tip plastic zone using local crack tip strain data obtained via high resolution SEM of loaded and unloaded cracks.

The fracture behavior of Al-Fe-X alloys was investigated with the objectives of identifying the micromechanisms of fracture and establishing microstructure/fracture property relationship. Tensile and J_{IC} tests were performed on four Al-Fe-X alloys at 316°C to characterize the yield stress, ultimate tensile strength, strain hardening exponent, local fracture strain, J_{IC}, K_{IC}, and the tearing modulus. The fracture mechanisms in the Al-Fe-X alloys were identified by sectioning unfractured J_{IC} specimens and examining the crack tip regions. Using micromechanical modeling, the origins of fracture toughness (K_{IC} and tearing modulus), or lack of toughness, in Al-Fe-X alloys were established and the brittle-to-ductile fracture transition were predicted. Potential means for improving the fracture resistance of Al-Fe-X alloys were discussed.

TABLE OF CONTENTS

I. RESEARCH OBJECTIVES

A. Task 1. Crack Tip Micromechanisms and Fatigue Lifetime Prediction

1. Perform detailed measurements and analysis of fatigue crack closure.

2. Investigate ways of including this information in models for fatigue crack growth.

B. Task 2. Microstructure/Property Relationships in Advanced Structural Alloys

1. Develop an understanding of the microstructure/property relationships in advanced Al-Fe-X alloys.

2. Identify the micromechanisms of fracture in dispersoid-hardened, powder-metallurgy Al alloys.

3. Devise a procedure for enhancing fracture toughness through microstructure modifications.

II. STATUS OF RESEARCH EFFORT

A. Task 1. Crack Tip Micromechanics and Fatigue Lifetime Prediction

1. Scope

During the past year, work has continued on the task of understanding fatigue crack growth, mainly through the use of micromechanics. In previous years, we have determined that fatigue cracks in several aluminum and titanium alloys exhibit the same characteristics of growth: (1) Direct observations of crack growth under high resolution conditions indicated that cracks do not grow on each cycle in the near threshold region. (2) Following an increment of growth, the crack is very sharp at maximum load but becomes progressively more blunt as damage is accumulated on each cycle prior to crack extension. (3) Crack growth rate correlates with the magnitude of strain attained at the crack tip. (4) Striations formed on the fracture surface do not correspond to one striation per cycle.

These general observations have been made for (1) large cracks (length > 1 mm), (2) small cracks (7 < length < 500 μm), during constant loading, and (3) for large cracks growing under simple variable amplitude loading. It must be concluded, therefore, that fatigue crack growth is occuring by the same basic mechanisms regardless of these differences. However, it is not possible to predict growth rates of cracks under these varying conditions of length and loading using the concepts linear elastic fracture mechanics. In fact, it is not even possible to predict the growth rates of large cracks under constant amplitude loading in the near-threshold region without invoking fatigue crack closure, even though the growth mechanism appears to be the same.

The most successful approach to predicting fatigue crack growth has been to correlate ΔK, the cyclic stress intensity factor computed from crack length and remotely applied stress, with crack growth rate, then to alter this "driving force" for crack growth using measurements of the crack closure. By this process, the "local driving force," usually denoted ΔK_{eff}, may be derived.

During the past year, we have used crack tip micromechanics to derive the local driving force for large and small fatigue cracks under constant amplitude loading and for large cracks under variable amplitude loading.

These results were derived for aluminum alloys for which previous work has provided an extensive data base. The conclusions derived from these analyses have now been extended to large and small fatigue cracks in a titanium aluminide alloy and a superalloy.

2. Current Status

a. Determination of Local Driving Force

Measurements of crack opening displacement (COD) near the crack tip have shown that in most cases, COD in Mode I varies as the square root of the distance behind the crack tip,

$$COD = Co\sqrt{y} \tag{1}$$

This is the same relation that would be expected from an elastic crack, except that the slope of the opening line has been found to be larger than would be predicted for an elastic crack at the imposed K level. The magnitude of strains surrounding the crack tip also indicate that the crack is not behaving in an elastic manner. This result is almost certainly another indication of the influence of crack closure, and is being further investigated.

The J integral concept developed by Rice has been applied to crack tips using measured displacements and strains near the crack, together with derived stresses [1,2]. This work found ΔJ, the cyclic equivalent to J, could be adequately represented by the relation

$$\Delta J = \delta \, \Delta\sigma \tag{2}$$

where δ = crack tip opening displacement and $\Delta\sigma$ = the stress range at the crack tip, as determined from strain at the crack tip and the cyclic stress-strain equation. The local driving force, $\Delta Keff^*$, is then determined from ΔJ using

$$\Delta Keff^* = (E\Delta J)^{1/2} \tag{3}$$

where E = Young's modulus. The problem in using eqs. (2) and (3) is in defining the crack tip opening displacement, δ. For the aluminum alloys, CTOD has been

defined as the opening 0.5 μm behind the crack tip.

b. Variable Amplitude Loading

Experiments were performed using the alloy 7091, and variable amplitude loading was simulated using overloads of several magnitudes and an overload/underload combination. Details of these experiments have been published [3]. Crack growth rates and crack tip parameters were measured before the overload and at several locations during the subsequent period of growth retardation. Table 1 shows the results of computing ΔKeff* for these cases.

Table 1
Derived Local Driving Forces

Analysis	da/dN (m/cy)	ΔKeff MPa√m	ΔKeff* MPa√m
1. ΔK = 6.9 MPa√m, R = 0.16, OLR* = 2.15			
Before OL	8.1×10^{-8}	3.5	5.3
+2550 cy	1.6×10^{-8}	3.9	4.2
+3550 cy	2.2×10^{-8}	2.1	3.6
2. ΔK = 6.0 MPa√m, R = 0.22, OLR* = 2.85			
Before OL	5.5×10^{-8}	2.6	4.2
+1200 cy	1.4×10^{-8}	0.8	3.9
+3500 cy	9.4×10^{-9}	1.2	3.8
3. ΔK = 7.2 MPa√m, R = 0.50, OLR* = 3.00, ULR* = 2.0			
Before OL	1.2×10^{-7}	4.9	7.2
+500 cy	1.0×10^{-7}	5.0	4.8
+2600 cy	5.0×10^{-8}	3.4	4.7

Also shown in the table for comparison are the values of ΔKeff determined using crack opening load, measured at the crack tip under high resolution conditions.

Crack growth rates for constant amplitude loading were then compared with those under variable amplitude loading using ΔKeff for constant amplitude loading and ΔKeff* for variable amplitude loading. This comparison is shown in Fig. 1, where it may be seen that ΔKeff* describes the local driving force

better than ΔKeff. The poorer correlation using ΔKeff is probably due to the variation in opening loads which occurs from cycle to cycle and the difficulty in measuring accurately the exact opening load.

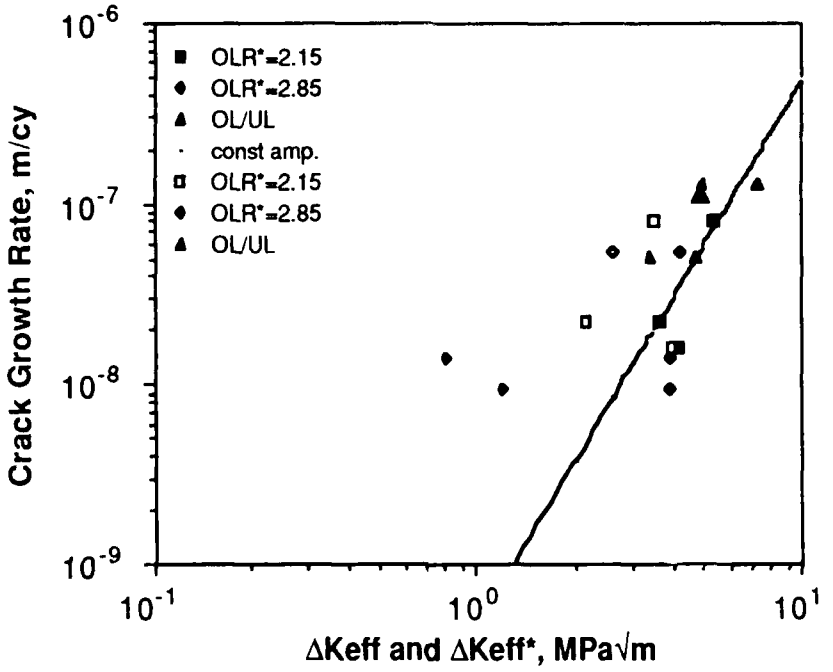

Fig. 1. Correlation between crack growth rate and crack driving force under variable amplitude and constant amplitude loading for 7091. Closed symbols are ΔKeff* and open symbols are ΔKeff. $OLR^* = \Delta K_{OL}/\Delta K$.

We have concluded from these results that crack growth rates after application of an overload, or overload/underload, cannot be predicted from constant amplitude loading data because the correct value of the crack driving force is unknown. There are no physically based models which adequately predict crack growth under variable amplitude conditions.

c. Correlation of Small and Large Crack Growth Rates

Local driving force values, ΔKeff*, have also been derived for large fatigue cracks in 7091, and for small and large fatigue cracks in 7075, all under

constant amplitude loading conditions. Crack closure values have also been measured for these cracks. These are shown in Fig. 2 for 7075.

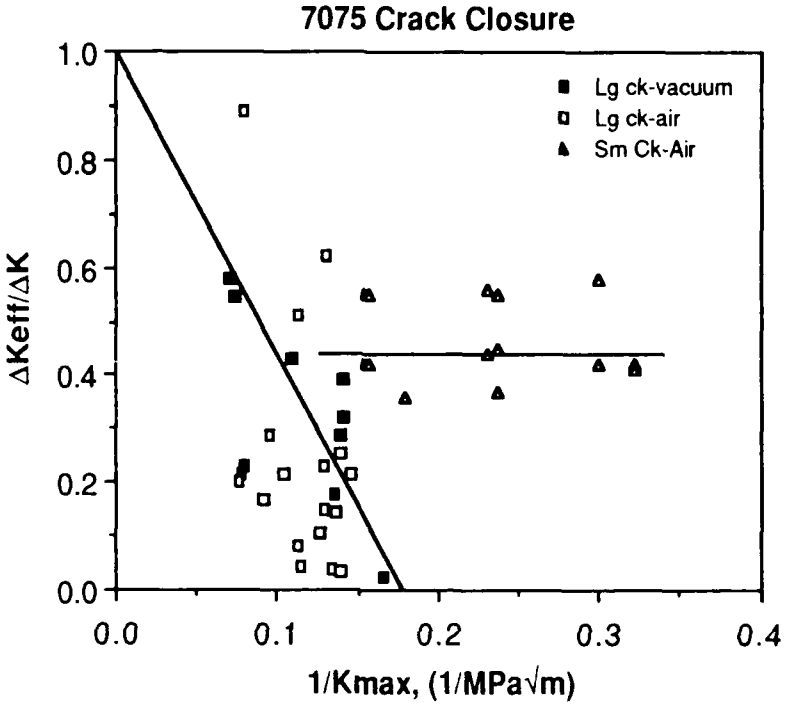

Fig. 2 Fatigue crack closure for large and small cracks in 7075 aluminum alloy. These data were determined at the crack tip under high resolution conditions.

A similar correlation has been found for large cracks in 7091 aluminum alloy and 304 stainless steel [3]. For these materials, the correlation was obtained over $0 < R < 0.8$, which provided a good test of the concept. Interpretation of the above figure is easiest at $R = 0$, where $\Delta K = K_{max}$. For this case, closure for large cracks may be written as

$$\Delta K_{eff} = \Delta K - \Delta K_{th} \tag{4}$$

while for small cracks, the appropriate relation is

$$\Delta K_{eff} = \beta \Delta K \tag{5}$$

where β = constant (≈ 0.4 for 7075). There is a fundamental difference in the

closure characteristics of large and small fatigue cracks. From Fig. 2, the transition between small crack and large crack closure behavior occurs at about $\Delta K = 10$ MPa$\sqrt{m}$, which corresponds to a crack length of about 150 μm for loading up to the yield stress.

The two different forms of eqs. (4) and (5) indicate that if ΔK_{eff}^* were to be determined using measured crack tip parameters in eq. (3), there should be a considerable difference in the effect of ΔK on the results. With the insight gained from the crack closure data from these alloys, the data base of crack tip parameters measured for aluminum alloys was reanalyzed so that ΔK_{eff}^* could be compared with the applied value of ΔK. The results of this comparison are shown in Fig. 3.

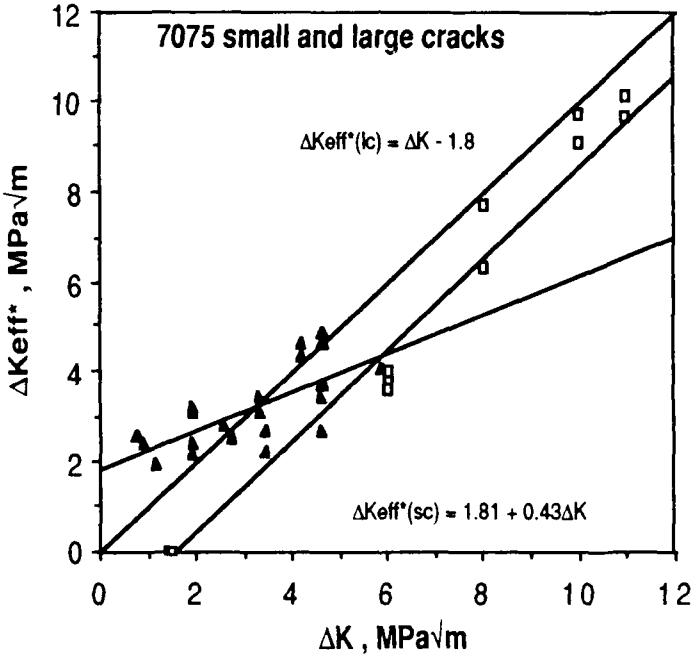

Fig. 3. Correlation between ΔK_{eff}^*, determined from measured crack tip parameters, and the applied ΔK.

The figure shows that the large crack data fit the form of eq.(4), but that for small cracks it is necessary to include an extra term in eq. (5),

$$\Delta K_{eff}^* = \Delta K_i + \beta \Delta K \qquad (6)$$

where the second term includes the applied ΔK less the crack closure. The origin of the ΔKi term is still being interpreted. However, it could be caused by fundamental differences between the behavior of small and large cracks. For small cracks, crack tip opening displacements and the levels of crack tip strain are larger than would be expected from similar measurements of these parameters for large cracks. Thus, ΔKi could be considered as that factor necessary to compensate for the "excess plasticity" at the tips of small cracks. Another way of describing the differences in small and large cracks is that the plastic zones of the small cracks are a significant fraction of the crack length, thus the small scale yielding assumption of linear elastic fracture mechanics, clearly valid for large cracks, is violated for small cracks. Another related observation is that the obvious geometric differences between small and large cracks cause the amount of constraint at the crack tip to be different, thereby altering the response of the material to the presence of the crack.

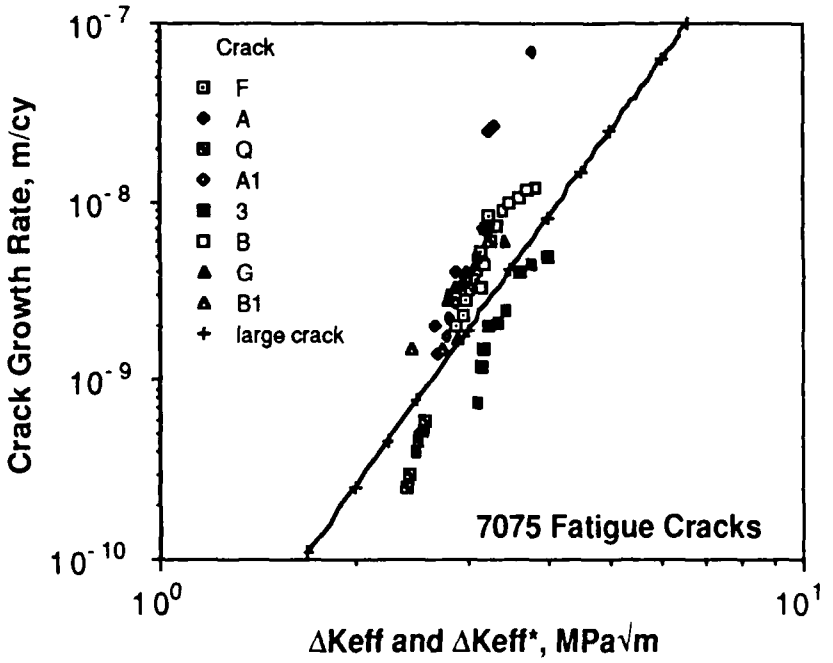

Fig. 4 Correlation between crack growth rates for large and small fatigue cracks. Crack closure and intrinsic plasticity terms are included for small cracks, whereas only crack closure is used for large cracks.

Final proof of the concepts described by eqs. (4) and (6) is whether crack growth data for large and small cracks can be correlated in terms of ΔKeff*. This correlation is shown in Fig. 4 for small and large cracks in 7075 alloy where crack closure and ΔKeff* has been determined for both large and small cracks. These data show a good correlation between small and large crack growth rates for nearly all of the cracks measured. A more complete development of these results has been accepted for publication in Acta Metallurgica [4].

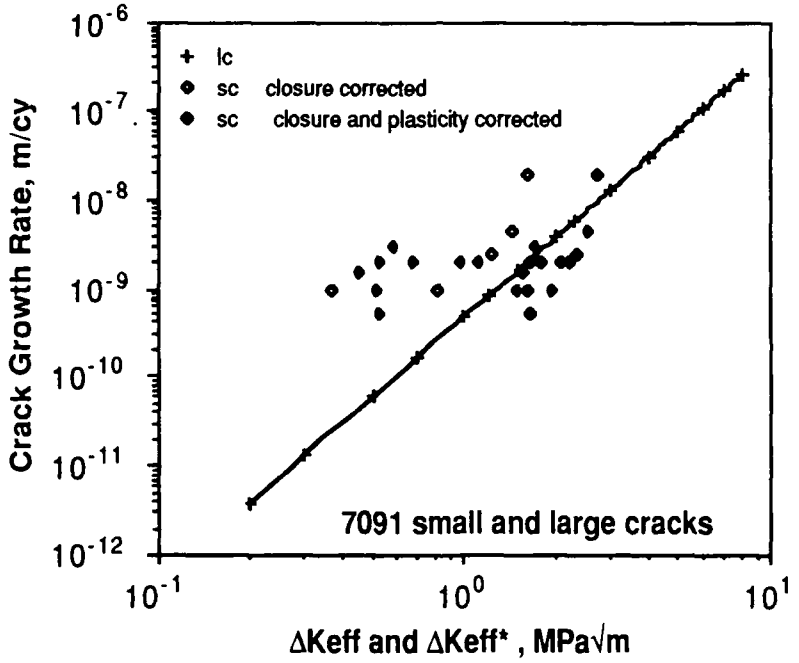

Fig. 5 Correlation between large and small fatigue crack growth rates. For small cracks, the correlation is shown altering ΔK for both closure and the plasticity.

In addition to the work on 7075, crack growth data have been obtained for both large and small fatigue cracks in 7091 aluminum alloy. This alloy, fabricated by powder metallurgy processing techniques, has a grain size of about 10 μm [5]. Therefore, it makes an interesting comparison to results for 7075, which has a large, pancake shaped grain structure [5]. However, ΔKeff* values for small cracks have not been measured for 7091 due to the difficulty of finding

microcracks in that microstructure. Rather, ΔKeff* has been estimated using a method for relating ΔKth and ΔKi worked out for 7075 [4]. The background for this method was given in last year's report and is further expanded in Ref. [4]. The procedure results in ΔKi ≈ 0.8 ΔKth. Crack growth rates correlated on the basis of ΔKeff for large cracks and ΔKeff* for small cracks are shown in Fig. 5.

These results again indicate that crack growth rates for small and large cracks correlate well when ΔKeff* is used as the driving force for small cracks. In addition, these results indicate that altering the applied ΔK to account for closure is insufficient to account for all the differences between large and small cracks.

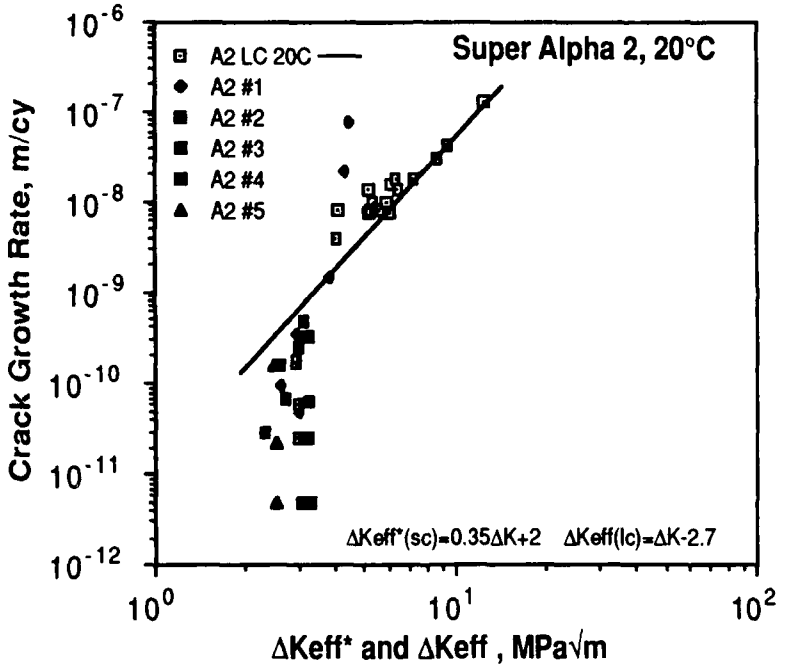

Fig. 6 Correlation between crack growth rate and ΔKeff for large and small cracks. For small cracks, ΔK has been both closure and plasticity corrected, while for large cracks, the only correction has been for closure.

Another example of using the procedure described above for estimating the driving force for small cracks from the ΔKeff of large cracks is shown in Fig. 6.

The material used for this example is the titanium aluminide alloy known as Super Alpha 2. Complete description of the microstructure of this material and more extensive results will be given in a forthcoming paper [6].

To obtain these results, closure has been estimated as $0.35\Delta K$ and $\Delta Ki = 2$ MPa$\sqrt{m}$. The locus of the fastest growth rates for these small cracks correlates well with results from the large crack. The reason some small crack growth rate points fall below and to the right of the line for the large crack is that the small cracks from which the data were collected were decreasing in growth rate as the cracks lengthened. Had the specimen not broken, it is likely that these cracks would have arrested.

A correlation between small and large fatigue crack growth rates using the same methods to measure closure and compute $\Delta Keff^*$ as described for 7075 has also been achieved in Astroloy, both at 20 and 600°C. This work will be available in report form within the next six months. Again, it was shown that altering ΔK to account for closure was insufficient, and that it was necessary to add the plasticity term to obtain a good correlation.

d. Conclusions

Careful study of the mechanisms of crack growth and the determination of the local driving force $\Delta Keff^*$ from measured crack tip parameters using eq. (3) have led us to conclude that crack growth rates can be correlated on the basis of $\Delta Keff^*$. This has been shown to be true for large cracks under variable amplitude loading in aluminum alloys, and for large and small cracks under constant amplitude loading in a variety of alloys.

The origins of plasticity induced closure have still have not been satisfactorily explained, nor has the correlation between ΔK and the crack growth rate.

B. Task 2. Microstructure/Property Relationships in Advanced Structural Alloys

1. Scope

Recent advances in alloy development and processing techniques have produced a new family of aluminum alloys, Al-Fe-X, which may be suitable for structural applications at service temperatures up to 340°C. Strengthened by a high volume fraction of thermally stable dispersoids, the Al-Fe-X alloys show good strength, high creep resistance, and adequate-to-moderate ductility at both room and elevated tempertures [1]. Unfortunately, the plane-strain toughness of some of the Al-Fe-X alloys is low ($\leq$ 10 MPa$\sqrt{m}$) [1] and must be increased considerably before structural uses of large extruded parts are feasible. The current program is aimed at improving the fracture toughness of Al-Fe-X alloys by developing a fundamental understanding of the fracture mechanisms in these dispersoid-hardened alloys. The efforts of the program are focused on (1) establishing microstructure/toughness relationships, (2) identifying origins of low fracture toughness, and (3) developing means for toughness enhancement of Al-Fe-X alloys.

2. Current Status

Four Al-Fe-X alloys of interest to the Air Force were selected for studies. The alloys selected and their manufacturers include: (1) Al-8Fe-7Ce (Alcoa), (2) Al-8Fe-2Mo-1V (Pratt & Whitney Aircraft), (3) Al-10.5Fe-2.5V (Allied-Signal), and (4) Al-8Fe-1.4V-1.7Si (Allied-Signal). Efforts in the last year were focused on characterizations of tensile properties, fracture toughness properties, and fractographic features of the four Al-Fe-X alloys at 316°C. The origins of fracture toughness and brittle-to-ductile fracture transition in Al-Fe-X alloys were examined on the basis of micromechanical modelling. These combined experimental and analytical efforts led to significant advances in the fundamental understanding of the microstructure/fracture property relationships in Al-Fe-X alloys, which will be discussed as follows: (a) characterization of microstructures, (b) characterization of tensile and fracture properties, (c) fracture mechanisms, (d) brittle-to-ductile fracture transition, (e) origins of toughness, and (f) discussion on toughness enhancement and future work.

a. Characterization of Microstructures

Optical and transmission electron microscopies were used to characterize the microstructures of the powder-metallurgy Al-Fe-X alloys. These efforts were initiated in the first year of this three-year program [2] and were continued in the last year characterizing the microstructure of the Al-8Fe-1.4V-1.7Si alloy. The size and distribution of Zone A particles and small dispersoids in the four Al-Fe-X alloys were determined by quantitative metallography using TEM thin foils or replicas. In the former case, the foil thickness was determined using the convergence beam technique. Table I summarizes the volume fraction and size range of the dispersoids in the Al-Fe-X alloys. Note that Al-Fe-Ce is the only alloy studied which contains a large volume fraction of Zone A particles. The various intermetallic phases (small dispersoids) present in these four Al-Fe-X alloys, compiled based on information reported in the literature [1,3], are also indicated in Table I. Most of the alloys in Table I contain intermetallic phases with incoherent interfaces in the Al matrix; the exception is the Al-Fe-V-Si alloy which is strengthened by coherent cubic α-silicide, $Al_{12}(Fe,V)_3Si$ [3].

b. Characterization of tensile and fracture properties

The tensile and fracture properties of Al-8Fe-1.4V-1.7Si were characterized by performing tensile and J_{IC} tests at both 25° and 316°C. Additionally, tensile and J_{IC} tests were also performed on the Al-Fe-Ce, Al-Fe-V, and Al-Fe-Mo-V alloys at 316°C. The J tests were used because some of the Al-Fe-X alloys (i.e., Al-Fe-V-Si at 25° and 316°C and Al-Fe-Mo-V at 316°C) were so ductile that valid K_{IC} tests could not be obtained using specimens of 7.6-12.7 mm thickness. The J tests provided information on the resistance of the material to crack initiation and growth in the forms of a J resistance curve, values of J_{IC} and tearing modulus, T_R.

Summaries of the tensile and fracture toughness properties of the four Al-Fe-X at 25° and 316°C are presented in Table II. The tensile properties reported in Table II include yield strength, ultimate tensile strength, strain hardening exponent (n), total elongation, and the local fracture strain, ε_{1f}, measured using tensile specimens photo-gridded with 0.5 mm diameter circles. The value of ε_{1f} was computed based on the

Table I. The Size and Volume Fraction of Intermetallic Dispersoids in Al-Fe-X Alloys

Material	Intermetallic Dispersoids	Volume Fraction, %	Diameter μm
Al-8Fe-7Ce	Zone A particles	13.0	1-10
	Al_8Fe_4Ce, Al_3Fe, $Al_{10}Fe_2Ce$, and precursor phases [1]	15.2	.15
Al-8Fe-2Mo-1V	$Al_{12}Fe(Mo,V)$, Al_6Fe, Al_3,Fe [1]	17.0	.1-1
Al-10.5Fe-2.5V	$Al_{10}V$ [3]	27.3	.2
Al-8Fe-1.4V-1.7Si	$Al_{12}(Fe,V)_3Si$ [3]	24.0	.025-.12

Table II. Tensile and Fracture Properties of Al-Fe-X Alloys at 25 and 316°C

Material	T, °C	Yield Stress MPa	σ_{uts}, MPa	n	Elongation, %	ε_{1f}#, %	K_{IC} MPa$\sqrt{m}$	Tearing Modulus T_R
Al-8Fe-7Ce	21°C	418.9	484.9	.053	7.0	15	8.5	0
	316°C	178.1	193.8	.050	7.6	28	7.9+	4.0
Al-8Fe-2Mo-1V	25°C	323.5	406.6	.084	6.7	18	9.0	0
	316°C	170.0	187.5	.043	7.2	27	8.1+	16.1
Al-10.5Fe	25°C	464.1	524.5	.036	4.0	8	5.7	0
-2.5V	316°C	206.3	240	.043	6.9	26	8.1+	1.3
Al-8Fe-1.4V	25°C	362.5	418.8	.085	6.0	41	36.4+	23.2
-1.7Si	316°C	184.4	193.8	.043	8.0	43	14.9+	7.4

Local fracture strain measured using tensile specimens gridded with 0.5 mm diameter circles

+ Computed from J_{IC} data using the expression: $K_{IC} = [EJ_{IC}/(1-\nu)^2]^{\frac{1}{2}}$

length of major axes of the circles and ellipses before and after deformation, respectively. The K_{IC} values were determined using standard K_{IC} tests or computed using the J_{IC} data obtained using standard J tests. All the K_{IC} data shown in Table II are for specimens tested in the LT orientation. Note that the K_{IC} value of the Al-Fe-X alloys at room temperature ranges from as low as 5.4 MPa$\sqrt{m}$ for Al-10.5Fe-2.5V to as high as 36.4 MPa$\sqrt{m}$ for Al-8Fe-1.4V-1.7Si. The K_{IC} values for the Al-Fe-Ce and Al-Fe-Mo-V alloys are $\approx$ 9 MPa$\sqrt{m}$. The J resistance curves of the four Al-Fe-X alloys are shown in Fig. 1. With the exception of the Al-Fe-V-Si alloy, the tearing modulus, T_R, of most of these alloys is nil at room temperature. The value of T_R increases with increase in test temperature for the Al-Fe-V, Al-Fe-Ce, and Al-Fe-Mo-V alloys.

c. Fracture mechanisms in Al-Fe-X alloys

The fracture mechanisms in the Al-Fe-X alloys at room temperture were previously studied by examining fracture tensile and K_{IC} specimens using optical and scanning electron microscopies, as well as Auger spectroscopy when necessary. These efforts were continued for all four Al-Fe-X alloys tested at 316°C. In addition, the fracture processes which occurred ahead of a growing crack in individual Al-Fe-X alloys were identified by arresting the crack in the J_{IC} specimen, sectioning the unfractured specimens, and examining the crack tip region using either optical or scanning electron microscopy.

The crack tip fracture processes in Al-Fe-X alloys are summarized in Fig. 2. At room temperature, the cracks in the Al-Fe-V, Al-Fe-Mo-V, and Al-Fe-Ce alloys are very sharp and without much crack tip blunting or any visible plastic fracture processes, as shown in Fig. 2(a) for the Al-Fe-Mo-V alloy. In LT-oriented Al-8Fe-2Mo-1V specimens tested at 316°C, the crack tended to propagate along the localized shear bands initially, but it also had a tendency to bifurcate and extend parallel to the loading direction due to the formation of longitudinal microcracks ahead of the main crack, as shown in Fig. 2(b). An arrested crack in Al-Fe-Ce alloy tested at 316°C, shown in Fig. 2(c), depicts a tendency to propagate along a path that goes through the matrix material, the matrix/Zone A particle interface, but seldomly through the Zone A particles. In the Al-Fe-V-Si alloys, the predominant fracture processes at both 25°

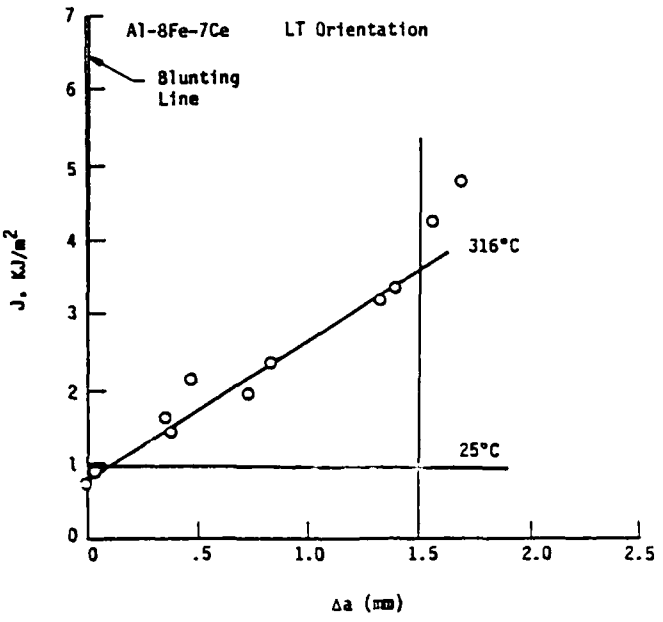

(a)

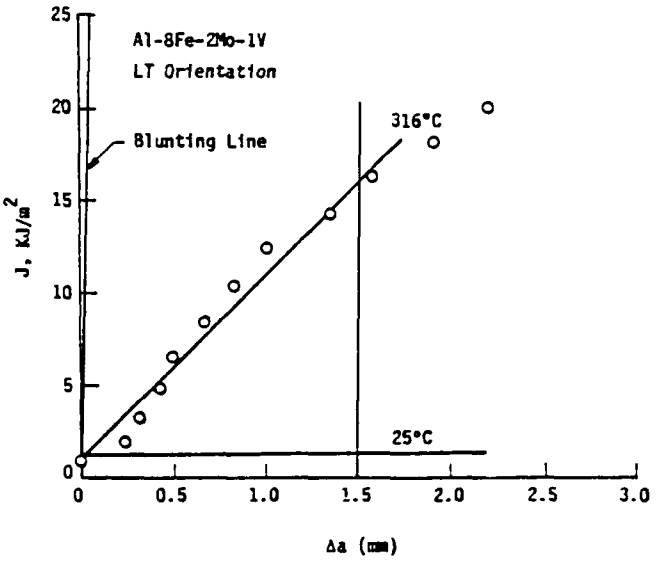

(b)

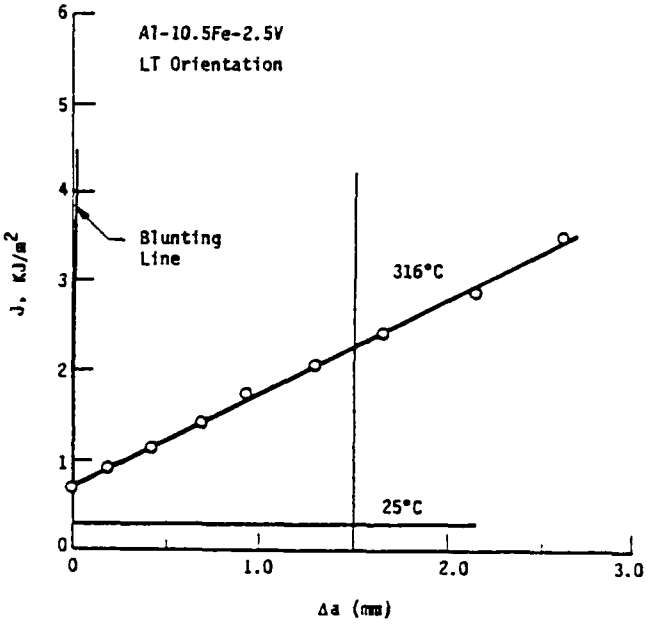

(c)

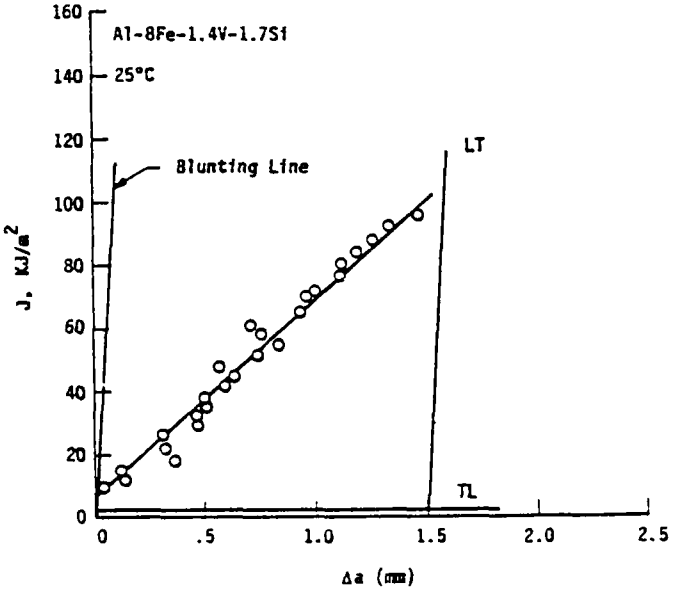

(d)

Figure 1. J Resistance Curves of Al-Fe-X Alloys at 25° and 316°C.

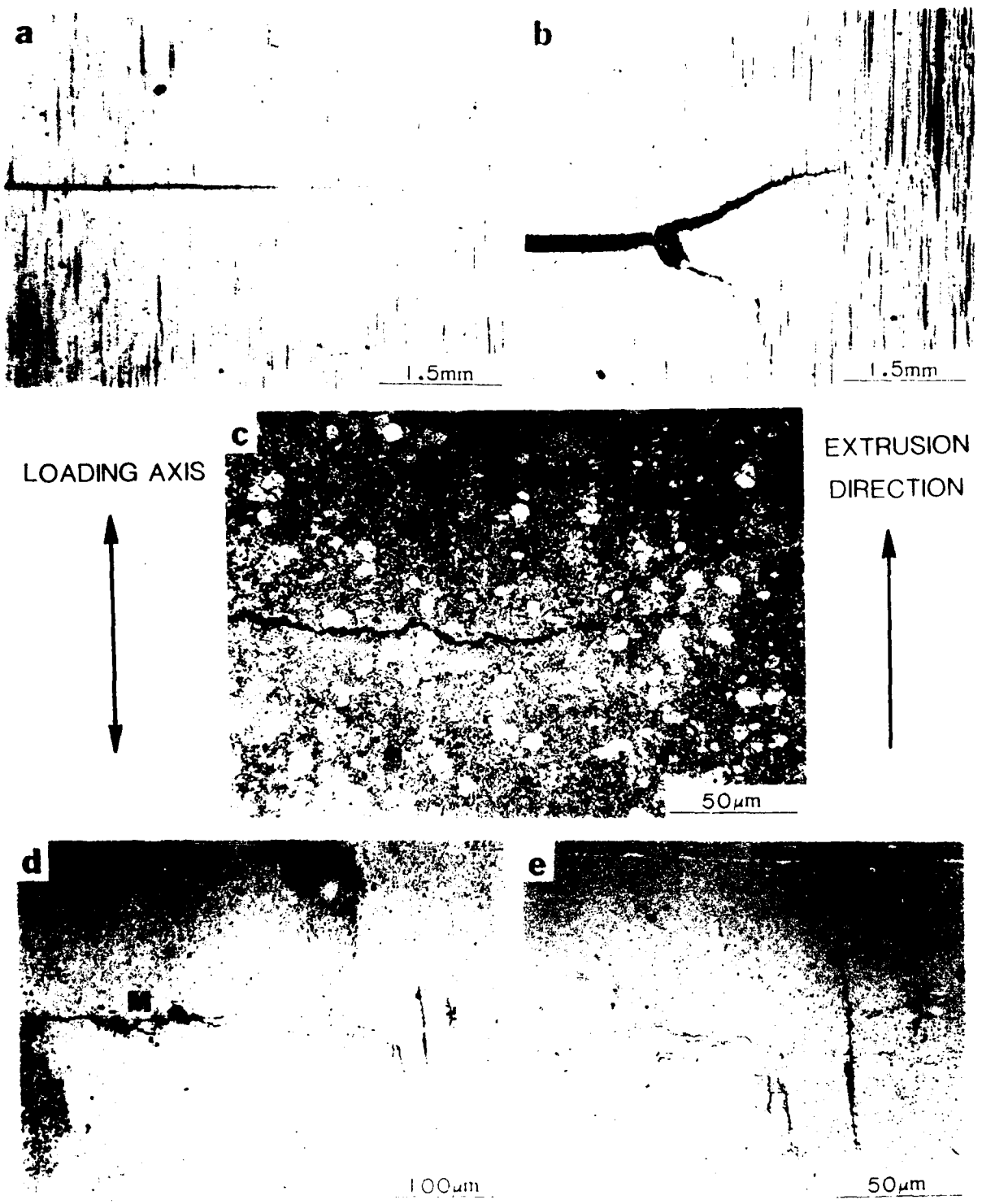

FIGURE 2. Fracture processes ahead the tip of arrested cracks in J test specimens: (a) sharp crack tip typically found in the Al-Fe-Mo-V, Al-Fe-Ce and Al-Fe-V alloys at 25°C; (b) crack propagation along a localized shear band and linkage with an internal microcrack in the Al-Fe-Mo V alloy at 316°C; (c) crack propagation through the matrix near the matrix/zone A particle interface in the Al-Fe-Ce alloy at 316°C; (d) and (e) linkage of the main crack (M) with microcracks ahead of the crack tip in the Al-Fe-V-Si alloy at 316°C.

and 316°C appeared to be the formation of microcracks and their eventual link-up with the main crack, Fig. 2(d). Microcracks were found to align either parallel to or normal to the loading axis, Fig. 2(e). There is also a tendency for the crack in a LT-oriented Al-Fe-V-Si specimen to bifurcate and propagate in a direction parallel to the loading axis.

As indicated earlier [2], the controlling fracture mechanisms in Al-Fe-Mo-V, Al-Fe-Ce, and Al-Fe-V alloys are nucleation of voids at 0.1-1 μm diameter dispersoids, which quickly coalesce to form cracks leading to final fracture. The lack of any observable microcracks or voids ahead of the sharp crack tip in Fig. 2(a) is consistent with that notion. One of the fractographic features in the compact-tension specimens of the Al-Fe-V-Si alloy tested at 25° and 316°C was the formation of thin sheet ligaments within the fracture process zone by internal delamination. At high magnification, the fracture surfaces of the Al-Fe-V-Si alloy exhibited dispersoid-initiated dimples. Fig. 3(a) and (b) show the thin sheet ligaments and dimple fracture surface in the Al-Fe-V-Si alloy tested at 25°C, respectively. The latter shows that dimples in the Al-Fe-V-Si alloy originated at small dispersoids in the range of 0.05-0.2 μm diameter. Thus, it appears that fracture of the Al-Fe-V-Si alloy is controlled by void nucleation at 0.05-0.2 μm diameter dispersoids. Once initiated, these voids quickly coalesced to form microcracks whose linkage with the tip of the main crack led to crack extension. Bifurcation of the main crack in specimens tested in the LT orientation was the consequence of preferred void nucleation at disperoids aligned in the TL orientation, resulting in TL-oriented microcracks which caused crack path deflection when linked with the main crack.

d. Brittle-to-ductile fracture transition

Fig. 1 clearly demonstrates that the resistance against stable crack growth varies greatly among the Al-Fe-X alloys. This is confirmed by the large differences in the value of the tearing modulus for the four Al-Fe-X alloys (Table II). Note that some of the Al-Fe-X alloys failed in a brittle manner at room temperture with a zero value of the tearing modulus. On the other hand, the LT oriented Al-Fe-V-Si alloy failed in a ductile manner, exhibiting a T_R value of ≈ 23.

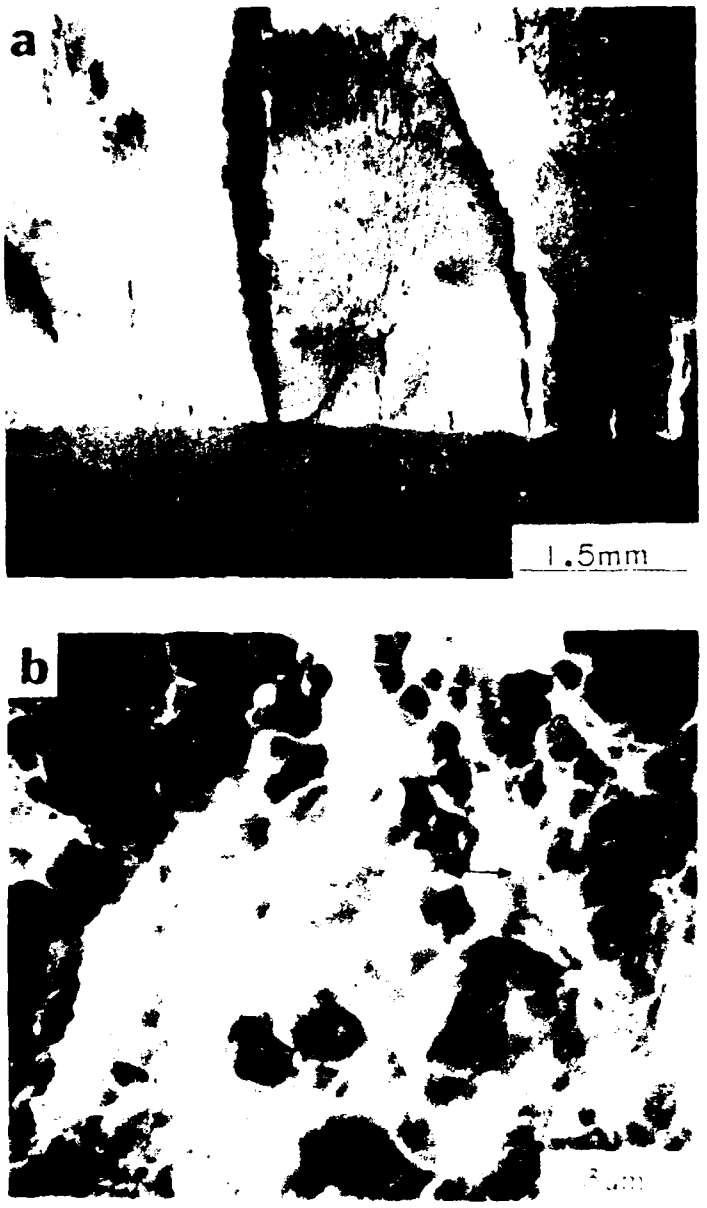

FIGURE 3. Fractographic features of Al-8Fe-1.4FV-1.7Si: (a) internal delamination and thin sheet ligaments in the fracture process zone, and (b) small dimples initiated at .06-.2 μm diameter dispersoids.

The brittle-to-ductile fracture transition observed in Al-Fe-X alloys was analyzed on the basis of mechanics of stable crack growth. The analysis indicated that the experimental tearing modulus is the consequence of the competition between the intrinsic tearing resistance of the material and the tearing stress induced due to crack extension, both of which can be quantified in terms of the normalized parameter, $\Omega = E\varepsilon_{1f}/\sigma_o$, where E, ε_{1f}, and σ_o are the elastic modulus, true fracture strain, and flow stress, respectively.

Some of the major findings of the micromechanical modelling efforts are: (1) a general expression for predicting the tearing modulus of a structural material based on the elastic modulus, true fracture strain, and flow stress (the average of the yield stress and ultimate tensile strength); (2) a new methodology for predicting brittle-to-ductile fracture transition. Comparison of the predicted tearing modulus with results of Al-Fe-X alloys, shown in Fig. 4, indicates good agreement between theory and experiment. A more extensive comparison of theory and experiment indicated the tearing moduli of a number of steels, Ni-, conventional Al-, and Ti-alloys are well-predicted over a wide range of Ω values.

The crack analysis also revealed that a critical value of Ω must be exceeded in order for $T_R > 0$ and ductile fracture to occur. That critical value of Ω was determined to be 34.5. This information was used to develop the concepts of tearing resistance curve and fracture mode diagram for depicting the transition of brittle-to-ductile fracture and vice versa. Fig. 5 shows comparison of the predicted brittle-to-ductile fracture transition boundary with experimental data of a number of structural alloys [4-6], including the Al-Fe-X alloys. Both Figs. 4 and 5 indicate that a critical value of intrinsic fracture strain must be exceeded in order for ductile fracture and a positive value of tearing modulus to occur.

e. Origins of fracture toughness in Al-Fe-X alloys

The critical strains at which void nucleation occurs in the Al-Fe-X alloys were determined recently via the following technique: (1) identifying the location where a void was first initiated in a tensile specimen using TEM replicas or scanning electron microscopy, and (2) obtaining the critical strain from

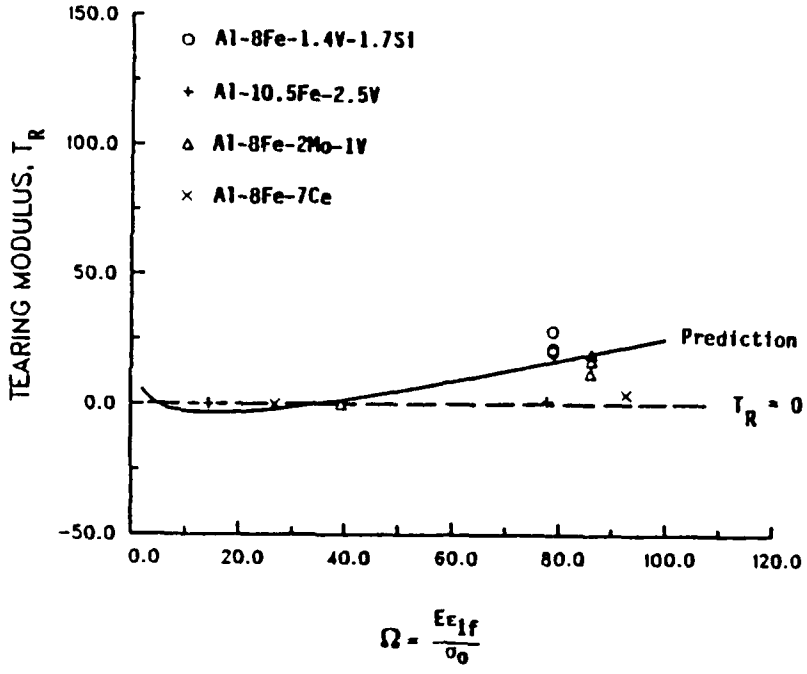

Figure 4. Comparison of the Predicted Tearing Resistance Curve With Experimental Data of Al-Fe-X Alloys

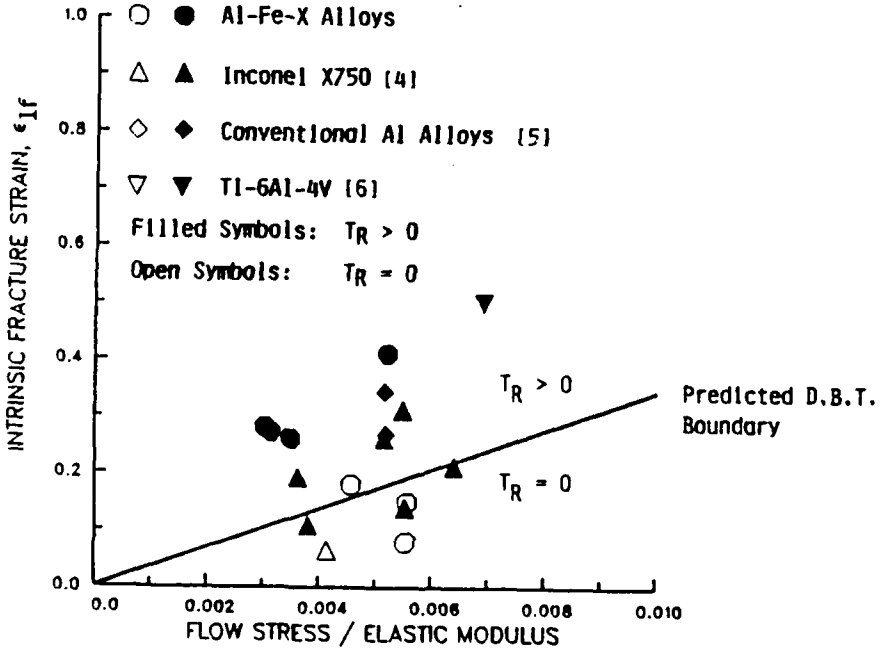

Figure 5. Comparison of the Predicted Ductile-to-Brittle Fracture Transition (D.B.T.) Boundary With Experimental Data of Al-Fe-X Alloys, Inconel X750, Ti-6Al-4V, and Conventional Al-alloys.

the strain distribution profile of the tensile specimen measured using the photo-grid method. At 25°C, the void nucleation strain is approximately equal to the fracture strain in the Al-Fe-X alloys. For the Al-Fe-Ce, Al-Fe-Mo-V and Al-Fe-V alloys which contain dispersoids in the size range of 0.1-1 μm, the void nucleation strains are about 8-18%. On the other hand, the nucleation strain for the Al-Fe-V-Si alloys, which contains ≈ 0.05 μm (.02 - .12 μm) diameter dispersoids, is 41% at 25°C as shown in Fig. 6. In addition to being smaller in size, the dispersoids in the Al-Fe-V-Si alloy are cubic α- silicides which are coherent with the matrix, as opposed to the incoherent dispersoids in the other three Al-Fe-X alloys.

Tanaka et al., [7] have previously demonstrated that the void nucleation strain in a dispersoid-hardened material increased with decreasing dispersoid size when decohesion is controlled by a strain-energy criterion. On the other hand, the void nucleation strain is independent of the dispersoid size when decohesion or fracture of dispersoids obeys a critical stress criterion. The transition from strain energy controlled decohesion to stress-controlled fracture occurs at a dispersoid size of ≈ .03 μm (Fig. 6). Since the dispersoids observed on the fracture surfaces of the Al-Fe-X alloys are approximately .06-1μm, fracture and/or interface debonding of these dispersoids are probably controlled by critical stress criteria. The increase in void nucleation strain observed in the Al-Fe-V-Si alloy is likely the consequence of a higher critical stress for either fracture of dispersoids or interface decohesion; the latter might be attributed to the coherent matrix/dispersoid interface. On the other hand, void nucleation in the other three alloys, despite also being stress-controlled, occurs at lower strain because of lower interface decohesion stresses resulting from larger dispersoid diameter and incoherent interface. Thus, the high fracture toughness of the Al-Fe-V-Si alloy is partly due to the ability of the microstructure to resist void formation at small dispersoids.

Another source of fracture resistance in some of the Al-Fe-X alloys arises from the formation of internal cracks by delamination along prior splat boundaries. This is observed in the Al-Fe-V-Si alloy at both 25° and 316°C, and in the Al-Fe-Mo-V alloy at 316°C. Delamination in those alloys resulted in thin sheet ligaments which are separated by surfaces free from normal

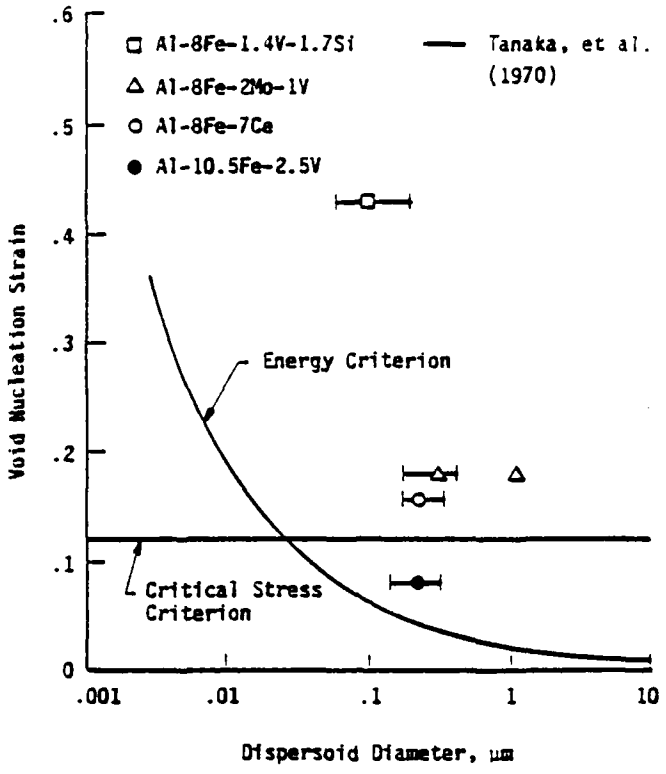

Figure 6. Void Nucleation Strain as a Function of Dispersoid Diameter.

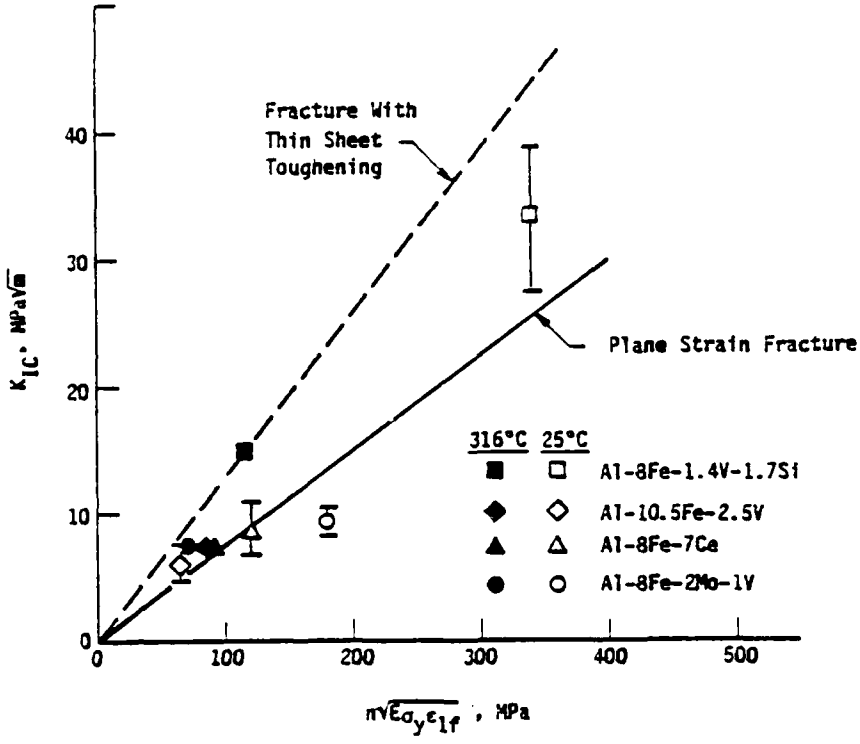

Figure 7. Comparison of Calculated and Experimental K_{IC} Results as a Function of $n\sqrt{E\sigma_y\varepsilon_{1f}}$. The dash line is model prediction, while the solid line is constructed based on results of the Al-Fe-Ce, Al-Fe-V, and Al-Fe-Mo-V alloys at 25°C.

stresses. Crack extension across the thin sheet ligament occurs under the plane-stress condition, as opposed to the plane-strain condition which would prevail had delamination not occurred. It is well known that the critical K value at fracture increases with decreasing specimen thickness [8] because of reduced plastic constraints and triaxial stresses. The relaxation of triaxial stresses ahead of the crack tip by internal boundary delamination in the process zone, referred to as thin-sheet effect, would increase the value of the fracture strain from $\varepsilon_{1f}/3$ (for plane strain) to that of ε_{1f} (for plane stress). This would lead to toughness enhancements (thin sheet toughening) by increasing the K_{IC} value (Fig. 7). The lack of stable crack growth in the Al-Fe-Ce, Al-Fe-Mo-V, and Al-Fe-V alloys at 25°C is due to low intrinsic fracture strain and the absence of thin sheet toughening and other shielding mechanisms, such as crack branching and deflection.

f. Discussion on toughness enhancement and future work

Based on the results of the last two years, it appears that high fracture toughness in Al-Fe-X alloys can be achieved as follows: (1) elimination of large, extraneous particles, such as Al-Fe intermetallic and stringer inclusions from the microstructure, (2) reduction of dispersoid size to less than 0.01 μm diameter to increase the void nucleation strain, (3) strengthening of the matrix with coherent dispersoids, and (4) manipulation of the microstructure to induce thin sheet toughening. This can be achieved by controlling the prior powder-particle or splat boundary strength through thermo-mechanical processing techniques to redistribute the broken oxide layers to some preferred and beneficial orientation to maximize thin sheet toughening (at the expense of transverse strength).

A very general scheme for enhancing the fracture toughness of brittle material and for predicting the brittle-to-ductile fracture transition was developed in the last reporting period. Future work in the coming year will be to extend this methodology to other state-of-the-art high temperature aluminum alloys, including SiC-strengthened Al alloy, the Al-Cr-Zr alloy produced by Alcan, and INCO MA aluminum alloys.

3. References

[1] S.L. Langenbeck, et al., "Elevated Temperature Aluminum Development," AFWAL-TR-86-4027, 1986.

[2] J. Lankford, et al., AFOSR Annual Report, Contract No. F49620-86-C-0024, 1987.

[3] D.J. Skinner, et al., "Dispersion Strengthened Al-Fe-V-Si Alloys," Scripta Met., Vol 20, 1986, pp 867-872.

[4] W.A. Logsdon, Advances in Cryogenic Engineering, Vol 22, 1977, pp 47-58.

[5] C.A. Griffis and G.R. Yoder, Trans. ASME, J. of Eng. Mat. and Tech., Vol 96, 1976, pp 152-158.

[6] G.R. Yoder and C.A. Griffis, ASTM STP 590, ASTM, Philadelphia, PA, 1976, pp 61-81.

[7] K. Tanaka, T. Mori, and T. Nakamura, "Cavity Formation at the Interference of a Spherical Inclusion in a Plastically Deformed Matrix," Vol 21, 1970, pp 267-279.

[8] D. Broek, Elementary Engineering Fracture Mech, Sigthoff & Noordhoff, The Netherlands, 1978, pp 181-214.

III. PUBLICATIONS (AFOSR SPONSORSHIP)

A. Task 1. Crack Tip Micromechanisms and Fatigue Lifetime Prediction

[1] "Plasticity Induced Fatigue Crack Closure,"--D.L. Davidson, ASTM-STP 982, Mechanics of Fatigue Crack Closure, J.C. Newman and W. Elber, eds, ASTM, Philadelphia, 1988, pp 44-61.

[2] "The Dependence of Crack Closure on Fatigue Loading Variables"--S.J. Hudak and D.L. Davidson, ibid., pp 121-138.

[3] "Microstructural and Fatigue Crack Tip Characterization of CORONA-5 and Powder Metallurgy Ti-6Al-4V"--D.L. Davidson, D. Eylon and F.H. Froes, in Microstructure, Fracture toughness and Fatigue Crack Growth Rate in Titanium Alloys, A.K. Chakrabarti and J.C. Chesnutt, eds., TMS-AIME, Warrenville, PA, 1987, pp. 19-37.

[4] "The Micromechanisms of Small Fatigue Crack Growth and the Influence of Metallurgical Factors"--J. Lankford and D.L. Davidson, Fatigue '87 EMAS Cradley Heath, UK, 1988 (in press).

[5] "Small and Large Fatigue Cracks in Aluminum Alloys"--D.L. Davidson Acta Metallurgica, 1988 (in press).

B. Task 2. Microstructure/Property Relationships in Advanced Structural Alloys

[1] "Fracture Mechanisms in Al-Fe-X Alloys,"--K.S. Chan, Dispersion Strengthened Aluminum Alloys, TMS-AIME, N.Y., edited by W.M. Griffith and Y.W. Kim, 1988 (in press).

[2] "Toughening By Thin Sheet Effects?"--K.S. Chan, Met Trans., 1988 (submitted).

[3] "A New Criterion for Brittle-To-Ductile Fracture Transition,"--K.S. Chan, Acta Meta., 1988 (submitted).

IV. PROGRAM PERSONNEL

Name	Title	
Dr. James Lankford	Institute Scientist	Co-Principal Investigators
Dr. David Davidson	Institute Scientist	
Dr. Gerald R. Leverant	Director, Materials Sciences	
Dr. K. S. Chan	Senior Research Engineer	
Mr. Forrest Campbell	Staff Technician	
Mr. Harold Saldana	Staff Technician	
Mr. John Campbell	Senior Technician	
Mr. James Spencer	Senior Technician	

V. INTERACTIONS--1987

A. Task. 1. Crack Tip Micromechanisms and Fatigue Lifetime Prediction

1. Presentation of paper at TMS meeting, Denver, CO, "Observations of Fatigue Crack Growth and Measurements of Crack Tip Plasticity in Titanium Alloys"--D.L. Davidson

2. Presentation of paper at TMS meeting, Denver, CO, "The Modeling of Fatigue Crack Growth Through Compressive Residual Stress Zones"--D.L. Davidson

3. "Fatigue Crack Growth," Seminar at Rice University--D.L. Davidson

4. Discussions at Materials Laboratory, Wright Aeronautical Laboratories, OH, About Fatigue Crack Growth in Metals and Composites

5. During the past year, the techniques developed, the insights into fatigue crack growth micromechanics, and the data collected and analyzed on this program have greatly benefited the work done on AFWAL Contract F33615-85-C-5051, Project 2420 "Growth of Small Fatigue Cracks in Aeroengine Disk Materials." Conversely, the information gathered on the AFWAL contract have benefited work done on this AFOSR contract.

B. Task 2. Microstructure/Property Relationships in Advanced Structural Alloys

Paper entitled,"Fracture Mechanisms in Al-Fe-X Alloys," by K.S. Chan was presented in the Symposium on Dispersion Strengthened Aluminum Alloys at the TMS-AIME meeting, Phoenix, AZ.

END

DATE

FILMED

6-1988

DTIC